Electron energy distributions from multiple ionization in 20–120-keV H^++Ar collisions

Yang-Soo Chung* and M. E. Rudd
Department of Physics and Astronomy, University of Nebraska, Lincoln, Nebraska 68588-0111
(Received 3 June 1996)

Energy-analyzed secondary electrons from H^++Ar collisions at eight proton energies from 20 to 120 keV were detected in coincidence with recoil ions of charge states 1–3. The charge states were distinguished by time-of-flight measurements and the electron energies were analyzed by a newly designed electrostatic analyzer of the low-pass high-pass filter type which has a large ($\sim 1.45\pi$ steradian) solid angle acceptance. For each of nine electron energies from 10 to 160 eV, the ionizing events associated with each residual ion charge state were counted. The electron energy dependence of the charge-state ratios and the average charge determined from the experimental data were in satisfactory agreement with calculations made with a simple statistical model based on the assumption of independent interactions between the projectile and the ejected electrons. In this model the single-electron ionization probability is assumed to be given by $P(b)=P(0)\exp(-b/r_0)$ where r_0 is a characteristic length and b the impact parameter. Values of r_0 amd $P(0)$ were determined by fitting the experimental data with this model. The charge-state ratios averaged over ejected electron energies agree with the data of DuBois *et al.* [Phys. Rev. A **29**, 70 (1984)]. [S1050-2947(96)09111-1]

PACS number(s): 34.50.Fa

I. INTRODUCTION

Multiple ionization of target atoms by proton impact has been studied by several investigators who measured the production of slow ions of various charge states. Examples of such studies are those of Solov'ev *et al.* [1], Wexler [2], Haugen *et al.* [3], DuBois, Toburen, and Rudd [4], and Hvelplund, Haugen, and Knudsen [5]. DuBois [6] and DuBois and Manson [7] analyzed this type of data to obtain information on the various mechanisms by which multiple ionization can occur. They showed that for H^++Ar collisions, capture plus ionization is the dominant mechanism below about 50 keV. Inner-shell ionization followed by the emission of Auger electrons is dominant for energies above 700 keV, but is not an important mechanism below 200 keV. Double capture is negligible, leaving multiple outer-shell ionization as the most important mechanism from about 50 to 700 keV.

More detailed information on multiple ionization can be obtained by measuring the relative population of the residual ion charge states as a function of the ejected electron energy. However, only two such measurements have been reported. Using 350 keV protons on helium, neon, and argon targets, Hippler, Bossler, and Lutz [8] made measurements of this type for electrons ejected at three different angles: 50°, 90°, and 120°. Except in spectral regions where Auger or Koster-Cronig electrons appeared, they found that a simple statistical model provided satisfactory agreement with their experimental results. Manzey [9] measured electrons at 90° emitted in coincidence with recoil ions of various charge states for 1-MeV He^+ impact on helium and neon. Electron spectra up to 120 eV were investigated for charge states 1 and 2 for helium and 1–3 for neon.

In the present experiment, we have extended the measurements of Hippler, Bossler, and Lutz to lower proton energies for H^++Ar collisions. However, instead of sampling the electron spectra at only a few angles, we utilized a newly designed and constructed low-pass high-pass filter analyzer with a much larger acceptance solid angle (4.6 sr, compared to Hippler's 0.015 sr), which collected electrons ejected over most of the range of polar angles. This allowed us to make direct measurements of relative cross sections that were differential only in the electron energy in coincidence with various charge states of the recoil ions. The use of this analyzer provided high electron and coincidence count rates resulting in relatively small statistical uncertainties. To compare this data with existing data on total ionization charge-state ratios, the differential charge-state ratios were averaged over electron energy with the appropriate weighting factor. Values of the average charge state were obtained separately for each electron energy and averaged over all electron energies. Measurements were made at eight proton energies from 20 to 120 keV.

II. IMPACT-PARAMETER DESCRIPTION OF MULTIPLE IONIZATION

The independent-interaction model for obtaining charge-state ratios as a function of the ejected electron energy, developed by Hippler, Bossler, and Lutz [8], was based on an impact-parameter formulation using the Massey adiabatic criterion. The singly differential cross section (SDCS) for a one-electron target is

$$\sigma(W)\equiv\frac{d\sigma}{dW}=2\pi bP(b)\,\frac{db}{dW}, \tag{1}$$

where W is the energy of the ejected electrons and $P(b)$ is the single-electron ionization probability as a function of the impact parameter b. The adiabatic criterion

*Present address: Joint Institute for Laboratory Astrophysics, Boulder, CO 80309.

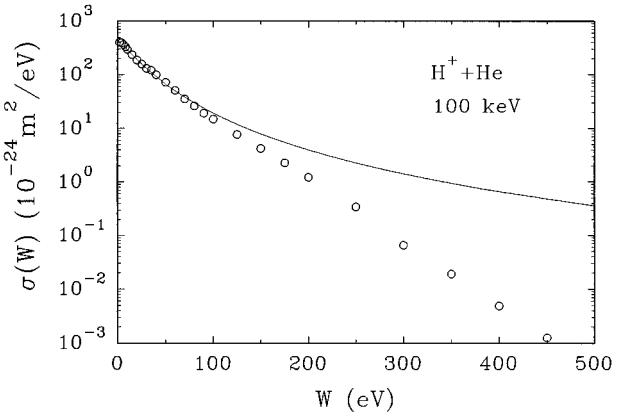

FIG. 1. Energy distribution of electrons from 100-keV H^++He collisions. Solid line, calculations from Eqs. (2)–(4); circles, experimental data [10].

$$b=\frac{2a_0\sqrt{RT}}{W+I} \tag{2}$$

is used to relate b to W, yielding the result

$$\sigma(W)=\frac{8\pi a_0^2 RT}{(W+I)^3}P(b), \tag{3}$$

where a_0 is the Bohr radius, I the binding energy of the electron, R the Rydberg of energy (13.6 eV), and $T=m_e v^2/2$, with m_e the electron mass and v the velocity of the incident particle. $P(b)$ is assumed to be an exponential:

$$P(b)=P(0)\exp(-b/r_0), \tag{4}$$

where r_0 is a characteristic length of the order of a_0 and $P(0)$ is the single-electron ionization probability for zero impact parameter.

For targets containing more than one electron, $\sigma(W)$ and $P(b)$ in Eq. (3) are replaced by $\sigma_n(W)$ and $P_n(b_n)$, which are the cross section and the probability for an n-fold ionization from a shell containing m electrons undergoing a collision at an impact parameter b_n. As pointed out by Hippler, Bossler, and Lutz [8], the appropriate value of the binding energy varies with n so the values of $\sigma(W)$, $P(b)$, I, and b are given subscripts. Assuming the interactions with the n electrons are independent, the probabilities are given by the binomial distribution

$$P_n(b_n)=\binom{n}{m}[P(b_n)]^n[1-P(b_n)]^{m-n}. \tag{5}$$

The charge-state ratios are

$$R_n(W)\equiv\frac{\sigma_n(W)}{\sigma_1(W)}=\frac{P_n(b_n)}{P_1(b_1)}\left(\frac{W+I_1}{W+I_n}\right)^3, \tag{6}$$

and the average charge associated with a given value of W is

$$\overline{n}(W)\equiv\frac{\Sigma n\sigma_n(W)}{\Sigma\sigma_n(W)}=\frac{\Sigma nR_n(W)}{\Sigma R_n(W)}, \tag{7}$$

where the summations are over the charge states.

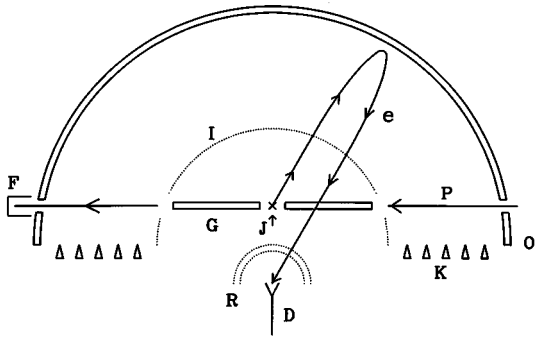

FIG. 2. Schematic diagram of the low-pass high-pass electron energy analyzer. *P*, projectile beam; *G*, beam guide; *F*, Faraday cup; *J*, Gas jet; *e*, typical electron trajectory; *I*, hemispherical grid; *O*, outer hemispherical electrode; *K*, guard rings; *R*, high-pass filter; *D*, electron detector.

In addition to questions about the validity of the assumption of independent interactions, this model can be criticized on the basis of its assumptions of adiabaticity and of an exponential ionization probability. A test of the model is shown in Fig. 1, in which Eqs. (2)–(4) were used to calculate SDCSs which are compared with experimental data for 100-keV H^++He collisions [10]. Double ionization was neglected since in helium it contributes very little to the cross section. Values of $P(0)$ and r_0 were chosen to give a fit at the lower values of W. While the shapes agree satisfactorily at low electron energies, the model fails badly at higher energies. Unfortunately, no other generally accepted method of relating the impact parameter to the ejected electron energy is known to us. And, as will be shown, whatever errors are inherent in this model when applied to cross sections evidently cancel out when charge-state ratios are calculated, since the agreement of the model with experimental ratios is quite good.

III. EXPERIMENTAL METHOD

A magnetically analyzed beam of protons with a beam diameter of 1.2 mm at the collision center passed through the target and was collected in a Faraday cup. The target was provided by argon gas effusing from a 1 mm aperture 1.5 mm below the beam. With the gas jet on, the pressure in the chamber rose to $\sim 10^{-6}$ Torr, but the pressure in the jet was not determined. Electrons ejected within a wide range of angles were energy selected by a low-pass high-pass electrostatic filter analyzer and detected in coincidence with residual ions which were charge selected using a time-of-flight (TOF) analyzer placed at 90° from the beam direction. Two layers of magnetic shielding inside the vacuum chamber reduced the magnetic field by a factor of 10. The addition of a single pair of exterior Helmholtz coils, oriented approximately with their axes along the direction of the Earth's magnetic field, reduced the residual field by another factor of 10. The resulting field, read by a rotating-coil gaussmeter, was uniform within 20% and less than 5 mG everywhere inside the chamber.

A. Electron energy analyzer

In order to obtain a relatively high coincidence count rate, we designed and built a hemispherical electrostatic analyzer

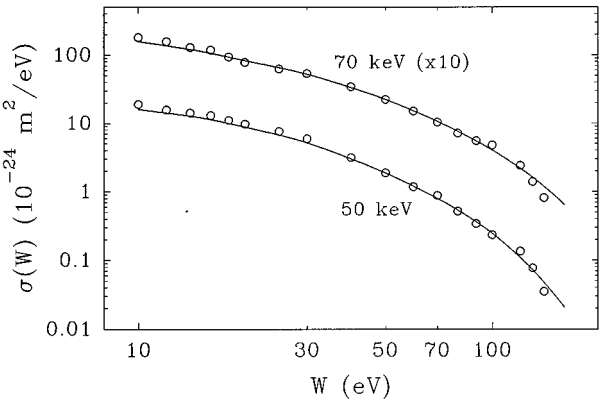

FIG. 3. Noncoincidence electron spectra from 50- and 70-keV H^-+Ar collisions. Solid lines, SDCS data from Rudd, Toburen, and Stolterfoht [14]; circles, relative SDCS data from this measurement normalized at 50 eV.

of the low-pass high-pass filter type similar in some respects to ones previously described [11]. Figure 2 shows a cross-sectional view of the apparatus. The proton beam P passed through the two sections of the rectangular beam guide G and into the Faraday cup F. The beam guide not only facilitated alignment, but also prevented electrons produced by collisions with the residual gas away from the collision center from reaching the detector. In addition, it provided a support for the gas supply tube. The target gas was injected at the collision center J. Electrons ejected from collisions at J traveled outward in a field-free region (a typical trajectory is shown as e) until they passed through the grounded hemispherical grid I. The outer hemispherical electrode O was at a potential $-(V+\delta V_1)$. Electrons with energies greater than $e(V+\delta V_1)$ reached the outer hemisphere where they were absorbed or scattered in random directions, while those with energies below that value were reflected back through the grid I, passed through the field-free region, and reached the electrode pair R, which formed the high-pass filter, and were detected at D. A retarding potential of $-(V-\delta V_2)$ between the grids at R passed electrons of energies above $e(V-\delta V_2)$. The overall resolution was then $\delta V=\delta V_1+\delta V_2$. Circular guard rings K held at the proper potentials by a resistor string reduced edge effects. The tube that carried the target gas to the jet also served to block electrons which would have been able to go directly from the collision center to the high-pass filter and detector.

Since the center of the large hemispheres was halfway between the collision center and the detector, electrons with energies within the pass-band of the analyzer were focused at D. The resolution of the analyzer was adjusted by varying the value of δV, while the nominal pass energy was determined by the value of V. The radius of the outer aluminum electrode O was 17.78 cm and that of the large grid I was 8.89 cm. Since the ratio of these radii was 2, the analyzer constant was unity, i.e., the electron energy (in eV) passed by the analyzer was equal to the potential (in volts) on the outer electrode. The ratio $r_1/r_2=0.286$ where r_2 was the radius of the grid I, and r_1 the distance from the center of the large hemispheres to the scattering center. Computer simulations of trajectories in the fields of this analyzer using the SIMION program [12] helped in optimizing the system. The

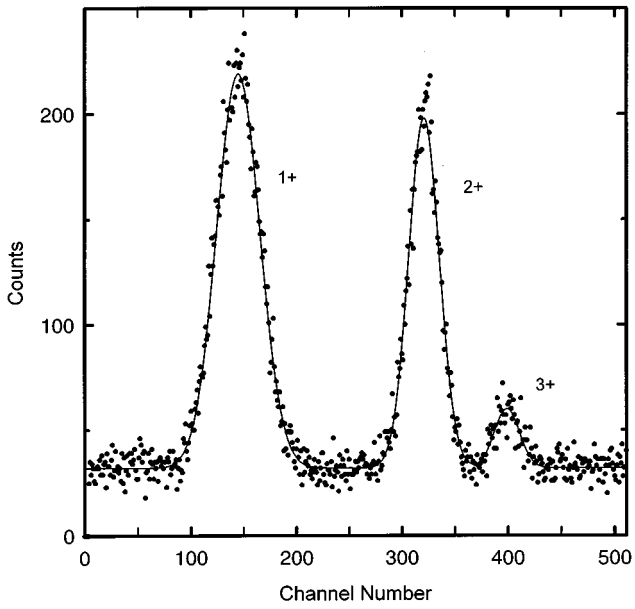

FIG. 4. Example of TOF coincidence spectrum for 50 eV electrons from 120-keV H^++Ar collisions.

resolution of the analyzer was degraded from its nominal value of $\delta V/V$ since the electron trajectories were not all perpendicular to the electrodes. The overall resolution was estimated to be about 0.5%.

The grids were made by stretching woven copper mesh over hemispherical aluminum forms. Each grid was then welded around its periphery to a copper ring while on the form. The 100-per-inch mesh had 0.002-in.-diam. wires. The grids were strengthened by electropolishing the wires to 0.001 in. and then plating them with chromium, bringing their diameters back to 0.002 in.. The grids and the outer electrode were covered with a thin coating of colloidal graphite to reduce contact potential differences and to increase their absorption of incident electrons.

The analyzer did not pass electrons emitted through the entire hemispherical solid angle of 2π sr because the collision center was, by necessity, not at the center of the hemispherical low-pass filter. This reduced the available solid angle to about 1.45π sr. As another consequence of the geometry, the fraction of electrons ejected at given angles that were able to reach the detector varied from zero for angles less than 16° or greater than 164° to about 41% at 90°. The overall efficiency was further reduced by the grid transmission fraction.

B. Time-of-flight ion charge-state analyzer

The TOF analyzer (not shown in Fig. 2) consisted of a shielded tube 125 mm long with grids at both ends followed by a Spiraltron electron multiplier (SEM) detector. The entrance of the TOF tube was 2–3 mm from the collision center. The slow argon ions were collected by a potential of -0.1 V and then accelerated through a potential difference of -100 to -150 V into the TOF drift tube to separate the charge states. The SEM was placed off axis so that it would not be exposed to photons from the collision region. A potential of -3000 V on the cone of the SEM attracted the ions leaving the TOF tube and also accelerated them to a suffi-

TABLE I. Charge-state ratios and average charge states for 20–60-keV H^++Ar collisions.

	20 keV			40 keV			50 keV			60 keV		
W (eV)	$R_2(W)$	$R_3(W)$	$\overline{n(W)}$	$R_2(W)$	$R_3(W)$	$\overline{n(W)}$	$R_2(W)$	$R_3(W)$	$\overline{n(W)}$	$R_2(W)$	$R_3(W)$	$\overline{n(W)}$
0[a]	0.089	0.0211	1.12	0.100	0.0156	1.12	0.113	0.0204	1.14	0.104	0.0145	1.12
10	0.134	0.0261	1.16	0.168	0.0317	1.19	0.180	0.0302	1.19	0.192	0.0285	1.19
15	0.156	0.0286	1.17	0.217	0.0302	1.21	0.185	0.0572	1.23	0.170	0.0386	1.20
20	0.180	0.0292	1.19	0.290	0.0484	1.27	0.199	0.0622	1.24	0.259	0.0407	1.25
30	0.168	0.0317	1.19	0.387	0.0524	1.31	0.239	0.0688	1.27	0.404	0.0520	1.32
50	0.193	0.0365	1.21	0.340	0.0609	1.30	0.314	0.125	1.36	0.503	0.0611	1.36
75	0.184	0.0531	1.22	0.484	0.0679	1.36	0.420	0.0923	1.36	0.467	0.0686	1.35
100	0.211	0.0607	1.25	0.496	0.0847	1.37	0.460	0.140	1.42	0.517	0.0847	1.38
130	0.240	0.0699	1.27	0.528	0.106	1.40	0.495	0.119	1.40	0.624	0.112	1.43
160	0.317	0.0865	1.32	0.533	0.113	1.40	0.493	0.159	1.44	0.742	0.132	1.46
Ave[b]	0.119	0.0247	1.15	0.191	0.0305	1.21	0.179	0.0445	1.22	0.213	0.0315	1.22

[a]Data at 0 eV are extrapolated values.

[b]Averages were calculated as described in Eqs. (9) and (12).

cient velocity to yield detection efficiencies of 41%, 50%, and 53%, respectively, for Ar^{1+}, Ar^{2+}, and Ar^{3+} ions. These values were obtained from the absolute efficiency measurements of DuBois for a channel electron multiplier [13]. Only relative values of these efficiencies were needed since we are reporting charge-state ratios. The intensity ratios $I(2+)/I(1+)$ and $I(3+)/I(1+)$ plotted as a function of the collection potential decreased rapidly at first but became constant for potentials larger than about 0.08 V so the value of 0.10 V was chosen for the measurements. The correspondingly small electric field near the collision center had no appreciable influence on the measurements of the electron spectra. Since the electron count rate was usually larger than the ion count rate, pulses from the ions were used as the start signals for the time-to-amplitude converter and delayed electron pulses as the stop signals.

C. Tests of the apparatus

It was found that the background count rate in the measured electron spectra rose rapidly above 140 eV, making measurements above 160 eV impossible. This background resulted from the large number of low- and intermediate-energy electrons which, while they could not traverse the high-pass filter, made collisions with gas molecules in its vicinity, producing positive ions. These were accelerated into the detector by the field of the filter. Lowering the potential of the high-pass filter had the expected effect of decreasing the background and increasing the signal, but it also degraded the resolution. Therefore, the measurements were limited to energies of 160 eV and below.

A noncoincidence measurement was made to test the operation of the electron system. Counts of ejected electrons measured at proton energies of 50 and 70 keV were converted into relative cross sections and compared with previous measurements [14]. Since the target density was not known, the relative SDCSs were normalized to the comparison data at 50 eV. As noted above, this system does not detect electrons ejected at angles less than 16° or greater than 164° and has a varying efficiency for the other angles. Thus, the results are not expected to be exactly the same as the

TABLE II. Charge-state ratios and average charge states for 70–120-keV H^++Ar collisions.

	70 keV			80 keV			100 keV			120 keV		
W (eV)	$R_2(W)$	$R_3(W)$	$\overline{n(W)}$	$R_2(W)$	$R_3(W)$	$\overline{n(W)}$	$R_2(W)$	$R_3(W)$	$\overline{n(W)}$	$R_2(W)$	$R_3(W)$	$\overline{n(W)}$
0[a]	0.0893	0.0132	1.11	0.0737	0.00975	1.09	0.065	0.00610	1.05	0.0279	0.00517	1.04
10	0.166	0.0212	1.17	0.143	0.0171	1.15	0.121	0.0132	1.13	0.100	0.00946	1.11
15	0.217	0.0322	1.21	0.154	0.0145	1.15	0.150	0.0583	1.21	0.164	0.00894	1.15
20	0.364	0.0388	1.29	0.254	0.0240	1.22	0.191	0.0256	1.19	0.213	0.0153	1.19
30	0.540	0.0560	1.37	0.412	0.0343	1.30	0.301	0.0368	1.26	0.446	0.0315	1.32
50	0.502	0.0586	1.35	0.469	0.0371	1.33	0.337	0.0526	1.29	0.483	0.0628	1.35
75	0.549	0.0699	1.38	0.455	0.0441	1.33	0.368	0.0482	1.30	0.442	0.0560	1.33
100	0.657	0.0901	1.42	0.543	0.0538	1.36	0.428	0.0653	1.34	0.390	0.0587	1.32
130	0.624	0.112	1.43	0.668	0.0658	1.40	0.549	0.0712	1.38	0.519	0.0565	1.36
160	0.798	0.118	1.45	0.718	0.0913	1.42	0.476	0.0860	1.37	0.570	0.0669	1.38
Ave[b]	0.229	0.0286	1.23	0.191	0.0192	1.19	0.146	0.0224	1.16	0.149	0.0153	1.15

[a]Data at 0 eV are extrapolated values.

[b]Averages were calculated as described in Eqs. (9) and (12).

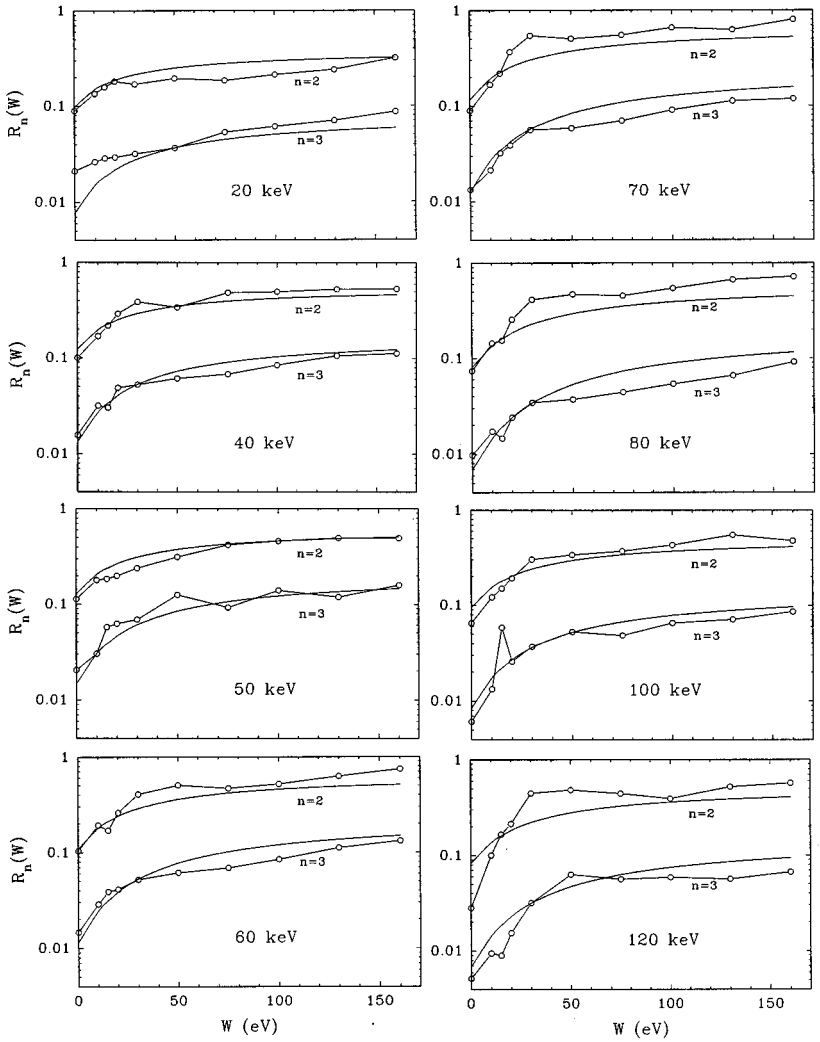

FIG. 5. Charge-state ratios as functions of W, the ejected electron energy. Points connected by lines, present data ($W=0$ values are extrapolated; see text); smooth curves, values calculated from Eq. (6).

previous electron spectra which resulted from numerical integration of data taken at discrete angles from 10° to 160°. Nevertheless, as shown in Fig. 3, the resulting spectral shapes were very similar.

IV. EXPERIMENTAL RESULTS

TOF spectra were obtained for all combinations of nine secondary electron energies and eight proton energies. An example is shown in Fig. 4 for 120 keV protons and 50 eV electrons showing well-defined peaks for the first three charge states. Each spectrum was fitted by the sum of three Gaussian functions and a constant. The relative areas of the peaks calculated from the fitting parameters and corrected for the different detector efficiencies yielded the charge-state ratios

$$R_n(W)=\frac{A_n(W)}{A_1(W)}, \tag{8}$$

where $A_n(W)$ is the area under the peak for charge state n at electron energy W. Values of $R_n(W)$ are listed in Tables I and II and are plotted as functions of secondary electron energy in Fig. 5. The general trend of the results is similar to those of Hippler, Bossler, and Lutz [8] and of Manzey [9]. Values of the average charge $\overline{n(W)}$ calculated using Eq. (7) are also given in the tables and are plotted in Fig. 6.

Using r_0 and $P(0)$ as adjustable fitting parameters, a least-squares fit of Eq. (6) was made to the products $R_2(W)R_3(W)$ of the experimentally measured ratios for all values of W. In this way, the values of the parameters were found that gave the best overall agreement of the spectra for all three charge states for each proton energy. Using the first three ionization potentials of argon and assuming that the binding energy was divided equally among the electrons emitted, we took $I_1=15.8$ eV, $I_2=43.4/2$ eV, and $I_3=84.3/3$ eV. The charge-state ratios and values of the average charge calculated from the resulting r_0 and $P(0)$ values are plotted in Figs. 5 and 6 where the agreement with experiment is seen to be fairly good. The 200 eV Auger peaks seen by Hippler, Bossler, and Lutz [8] are above our measured range of electron energies. The 40 eV Coster-Kronig peaks, conspicuous in their graphs, are less prominent in our data taken at lower incident particle energies and disappear at the lowest energies. The values of r_0 and $P(0)$ are plotted vs incident energy in Fig. 7, where r_0 is seen to be approximately constant, a condition necessary for the validity of the independent interaction mechanism given by DuBois and Manson [7]. However, the large uncertainties resulting from the fitting indicate that this is not an accurate method of determining r_0. Furthermore, our values of r_0 are somewhat higher than their data.

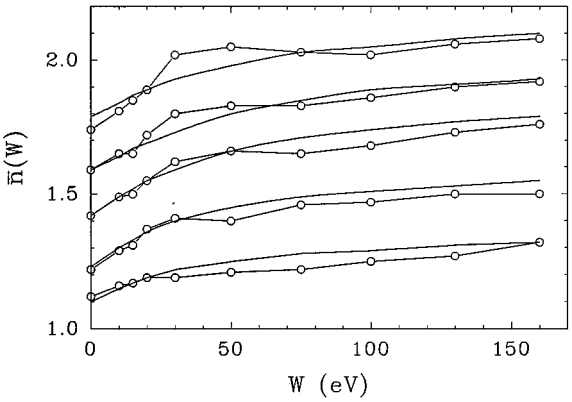

FIG. 6. Comparison of experimental and calculated values of $\overline{n(W)}$ vs W. From bottom to top, proton energies are 20, 40, 60, 80, and 120 keV. Values at energies above 20 keV have been shifted upwards by successive amounts of 0.1 to avoid overlap.

To compare to charge-ratio data of other investigators taken without electron energy selection, a weighted average of $R_n(W)$ must be made:

$$R_n \equiv \frac{\sigma_n}{\sigma_1} = \frac{\int \sigma_n(W)dW}{\int \sigma_1(W)dW} = \frac{\int R_n(W)\sigma_1(W)dW}{\int \sigma_1(W)dW}. \quad (9)$$

The cross section $\sigma_1(W)$ can be obtained from

$$\sigma_1(W) = \frac{\sigma(W)}{\Sigma n R_n(W)}, \quad (10)$$

where

$$\sigma(W) = \sum n\sigma_n(W) \quad (11)$$

is the ordinary SDCS measured without discrimination of the residual ion charge state. Because of the preponderance of low-energy electrons in the spectrum, R_n tends to reflect the values of $R_n(W)$ at low electron energies. The average over W of $\overline{n(W)}$ is

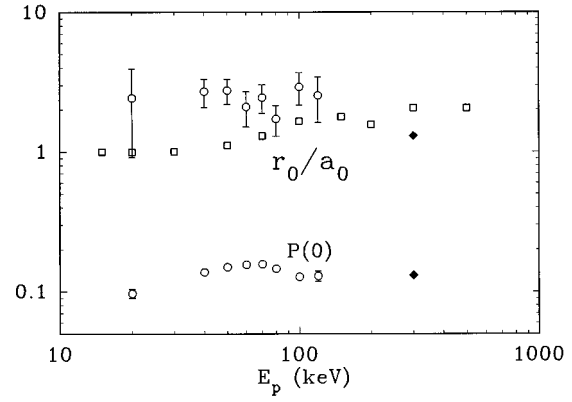

FIG. 7. Values of r_0/a_0 and $P(0)$. Circles with error bars, results obtained by fitting Eq. (6) to the charge-state ratio data; squares, averages of 2+ and 3+ data of DuBois and Manson [7]; black diamonds, data of Hippler *et al.* [8].

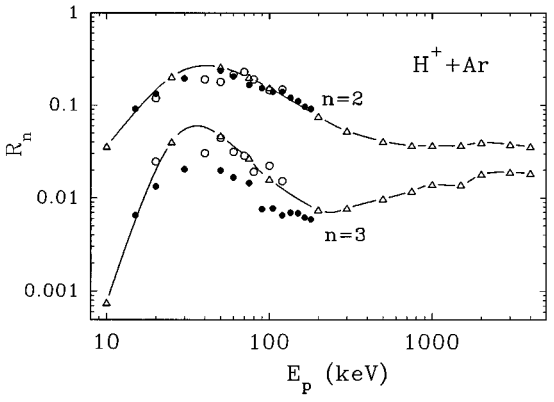

FIG. 8. Charge-state ratios averaged over W. Open circles, this data; triangles with lines, data of DuBois, Toburen, and Rudd [4]; filled circles, data of Solov'ev *et al.* [1].

$$\overline{n} = \frac{\Sigma \overline{n(W)}\sigma_n(W)}{\Sigma \sigma_n(W)} = \frac{\Sigma \overline{n(W)}R_n(W)}{\Sigma R_n(W)}. \quad (12)$$

The average charge state is of importance since it can readily be shown that

$$\overline{n} = \frac{\sigma_{\text{ion}}}{\sigma_{\text{count}}}, \quad (13)$$

where the quantity σ_{ion} is the total ionization cross section, obtained by measuring the total charge of ions produced, while σ_{count} is the ''counting'' ionization cross section that results from counting ionizing events.

Values of R_n and $\overline{n}$ calculated from Eqs. (9) and (12) are also given in the tables. Since the lack of data below 10 eV would distort the average, we made an extrapolation of the $R_n(W)$ values to 0 eV to obtain more accurate averages. Since experimental values of $\sigma(W)$, needed in Eq. (10), were not available at all of the proton energies, those cross sections were calculated from the analytical model given by Rudd [15]. Figure 8 shows a comparison of these R_n values with those of DuBois, Toburen, and Rudd [4] and Solov'ev *et al.* [1]. Values of $\overline{n}$ calculated from Eq. (12) are compared in Fig. 9 with those of DuBois, Toburen, and Rudd [4] and of

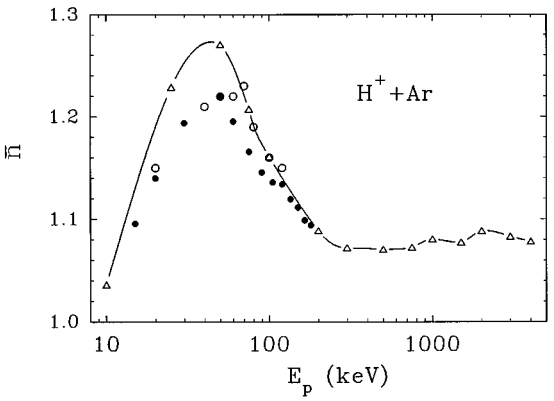

FIG. 9. Average charge $\overline{n}$ [values of $\overline{n(W)}$] averaged over W. Symbols as in Fig. 8.

Solov'ev *et al.* [1]. Our results agree well with the former data for 70 keV and above, but better with the latter at 50 keV and lower.

V. CONCLUSIONS

Our measurements of recoil-ion charge-state ratios as a function of ejected electron energy are compared to the results of calculations using a simple statistical model based on the binomial distribution, the adiabatic relation, and the assumption of an ionization probability which decreases exponentially with impact parameter. While the assumptions of the model can be criticized, it fits the experimental charge-ratio data fairly well even at energies below 50 keV, where capture plus ionization dominates. This indicates that the energy distribution of ejected electrons is approximately the same whether a second (or third) electron removed in the same collision is captured by the projectile or emitted into the continuum. It would be desirable to test the model over a wider range of proton and electron energies.

ACKNOWLEDGMENTS

We wish to thank R. DuBois for helpful consultations and for furnishing values of detector efficiencies and D. Jaecks, T. Gay, and K. Trantham for useful suggestions. This material is based on work supported by the National Science Foundation under Grant Nos. PHY9020529 and PHY9119818.

[1] E. S. Solov'ev, R. N. Il'in, V. A. Oparin, and N. V. Fedorenko, Zh. Eksp. Teor. Phys. **42**, 659 (1962) [Sov. Phys. JETP **15**, 459 (1962)].

[2] S. Wexler, J. Chem. Phys. **41**, 1714 (1964); **44**, 2221 (1966).

[3] H. K. Haugen, L. H. Andersen, P. Hvelplund, and H. Knudsen, Phys. Rev. A **26**, 1962 (1982).

[4] R. D. DuBois, L. H. Toburen, and M. E. Rudd, Phys. Rev. A **29**, 70 (1984).

[5] P. Hvelplund, H. K. Haugen, and H. Knudsen, Phys. Rev. A **22**, 1930 (1980).

[6] R. D. DuBois, *X84 International Conference on X-Ray and Inner-Shell Processes in Atoms, Molecules, and Solids*, edited by A. Meisel and J. Finster (Karl-Marx-Universität, Leipzig, Zwickau, 1984).

[7] R. D. DuBois and S. T. Manson, Phys. Rev. A **35**, 2007 (1987).

[8] R. Hippler, J. Bossler, and H. O. Lutz, J. Phys. B **17**, 2453 (1984).

[9] D. Manzey, Diplomarbeit, J. W. Goethe Universität Frankfurt/M, 1991 (unpublished).

[10] M. E. Rudd, L. H. Toburen, and N. Stolterfoht, At. Data Nucl. Data Tables **18**, 413 (1976).

[11] J. D. Lee, Rev. Sci. Instrum. **44**, 893 (1973); Hiroshi Daimon, *ibid*. **59**, 545 (1988); Hiroshi Daimon and Shozo Ino, *ibid*. **61**, 57 (1990).

[12] The SIMION program, which calculates charged particle trajectories in electric and magnetic fields of specified configurations, is available from David A. Dahl, MS 2208, EG&G Idaho Inc., Idaho National Engineering Laboratory, P.O. Box 1625, Idaho Falls, ID 83415.

[13] R. D. DuBois, Phys. Rev. A **36**, 2585 (1987), and private communication. Note that the value 0.01 on the *y* axis of his Fig. 2(b) should be 0.03.

[14] M. E. Rudd, L. H. Toburen, and N. Stolterfoht, At. Data Nucl. Data Tables **23**, 405 (1979).

[15] M. E. Rudd, Phys. Rev. A **38**, 6129 (1988).